Supporting Information

Local Hydroxide Ion Enrichment at Inner Surface of Lacunaris Perovskite Nanotubes Facilitates Oxygen Evolution Reaction

Lin-Bo Liu,[†] Shuo Liu,[†] Yu-Feng Tang,[†] Yifei Sun,[§] Xian-Zhu Fu,[#] Jing-Li Luo,[#, ‡] Subiao Liu[†, *]

[†]School of Minerals Processing and Bioengineering, Central South University, Changsha, Hunan 410083, China

[§]College of Energy, Xiamen University, Xiamen, Fujian 361005, China

[#]College of Materials Science and Engineering, Shenzhen University, Shenzhen, Guangdong 518055, China

[‡]Department of Chemical and Materials Engineering, University of Alberta, Edmonton, Alberta T6G 1H9, Canada

Corresponding author: Subiao Liu

Telephone: +1 780 492 2232

E-mail: subiao@csu.edu.cn

Specifications of chemicals:

Polyvinylpyrrolidone (PVP, M_w ~1300000), N, N-Dimethylformamidel (DMF, 99.5%), ethylenediamine tetraacetic acid (EDTA, 99.5%), citric acid (99.5%), $Pr(NO_3)_3 \cdot 6H_2O$ (99%) were purchased from Macklin company. Isopropanol (99.7%), $Sr(NO_3)_2$ (99.5%), $Ni(NO_3)_2 \cdot 6H_2O$ (98%) were purchased Sinopharm Chemical Reagent Co. Lt. $La(NO_3)_3 \cdot 6H_2O$ (98%), $Ba(NO_3)_2$ (99.5%) were purchased form FuChen Chemical reagent o. Lt. $Co(NO_3)_2 \cdot 6H_2O$ (98.5%), $Fe(NO_3)_3 \cdot 9H_2O$ (98.5%) were purchased form Guanghua Technology Co. Lt. NH_3H_2O (25-28%) were purchased form Chuandong Chemical Co. Lt. Nafion perfluorinated ion-exchange resin solution (5 wt.% in mixture of lower aliphatic alcohol & H_2O), IrO_2 powder (99%) were purchased from Alfa Aesar.

Material Synthesis:

The mesoporous $La_{0.5}Pr_{0.25}Ba_{0.25}Co_{0.8}Ni_{0.2}O_{3-\delta}$ nanotubes (LPBCN-NTs) were prepared via electrospinning method followed by calcination process. Typically, 0.75 mmol $La(NO_3)_3 \cdot 6H_2O$, 0.375 mmol $Ba(NO_3)_2$, 0.375 mmol $Pr(NO_3)_3 \cdot 6H_2O$, 1.2 mmol $Co(NO_3)_2 \cdot 6H_2O$ and 0.3 mmol $Ni(NO_3)_2 \cdot 6H_2O$ were dissolved in 10 mL DMF, then ~1.41 g PVP powders (15wt% relative to DMF) was added slowly into the above solution, which was further stirred overnight at room temperature to ensure the full mix of metal precursors and polymer. The obtained metal salts-polymer solution was loaded into a plastic syringe equipped with a 22-G needle for electrospinning. The applied voltage and distance between the needle tip and the collector were fixed at 20 kV and 15 cm, respectively. The feeding rate for the precursor solution was controlled as 5 μL min^{-1}. Then, the obtained metal salts-polymer fibers were calcined under air at 750 ºC for 2 h with heating rates of 2 ºC min^{-1}.

$La_{0.5}Pr_{0.25}Ba_{0.25}Co_{0.8}Ni_{0.2}O_{3-\delta}$ nanofibers (LPBCN-NFs) were prepared by the same method described above except that the volume of DMF was 9 mL.

LPBCN and $Ba_{0.5}Sr_{0.5}Co_{0.8}Fe_{0.2}O_{3-\delta}$ nanoparticles (denoted as LPBCN-NPs and BSCF, respectively) were synthesized using a modified sol-gel method. Stoichiometric amounts of $La(NO_3)_3 \cdot 6H_2O$, $Ba(NO_3)_3$, $Pr(NO_3)_3 \cdot 6H_2O$, $Co(NO_3)_2 \cdot 6H_2O$, $Ni(NO_3)_2 \cdot 6H_2O$ (or Stoichiometric amounts of $Ba(NO_3)_2$, $Sr(NO_3)_3$, $Co(NO_3)_2 \cdot 6H_2O$, $Fe(NO_3)_3 \cdot 9H_2O$) were dissolved in EDTA-NH_3H_2O combined solution under continuous heating and stirring, then citric acid was introduced into the above solution. The molar ratio of EDTA acid: citric acid: total metal ions was controlled to be around 1: 1.5: 1. Subsequently, NH_3H_2O was added to adjust the pH value to around 8. The solution was stirred and heated on a hot plate at 80 °C until the formation of organic resins containing the homogeneously distributed cations because of the slow evaporation of the solvent. The synthesized gel was decomposed at 300 °C for 4 h to remove the organic components and the nitrates. The precursor powders were then calcinated in air to obtain the perovskite particles.

Materials Characterization:

The crystalline structure of all the synthesized powders was identified by XRD with Rigaku Rota flex Cu Kα radiation (40 kV, 44 mA) and the raw data were analyzed with JADE version 6.5. Microstructures were determined with a high-resolution Zeiss Sigma field emission scanning electron microscope (FESEM) equipped with an EDX detector. The low- and high-resolution transmission electron microscopy (TEM) images were acquired by using a Thermo Scientific Talos F200X STEM. The TEM uses an electron beam as light source (Lab6 crystal in this case) and the beam goes through (transmission) the specimen. The TEM was operated at an accelerating

voltage of 200/300 kV. Images were achieved using a Gatan digital imaging system through Digital Micrograph software. The N_2 adsorption-desorption isotherms were measured using an Autosorb Quantachrome 1Q apparatus. X-ray photoelectron spectroscopy (XPS, Kratos AXIS Ultra) was used to investigate the surface chemistry of the LPBCN-NTs, LPBCN-NFs and LPBCN-NPs with the adventitious carbon (C 1s) at the binding energy (BE) of 284.8 eV as the reference. The solid–liquid contact was recorded on a DROPMETER A100P instrument (MAIST). FTIR spectra were characterized on a NicoletNexus 470 spectrophotometer (THERMO).

d-spacing Calculation:

The XRD pattern can be used to determine the interplanar spacing (*d*-spacing) using Bragg's law:

$$n\lambda = 2d\sin\theta$$

where n is the order of diffraction, λ is the wavelength of the incident X-ray. For Cu Kα radiation, λ = 1.5406 Å; *d* is the interplanar spacing and θ is the angle of diffraction. The d spacing of LPBCN-NT (110) was calculated as follows:

$$d = \frac{n\lambda}{2\sin\theta} = \frac{1.5406}{2 * \sin 16.4} = 2.73 \text{ Å}$$

Oxygen Vacancy Content Determination:

The oxygen vacancy content was measured using an iodometric titration method under the Ar atmosphere [S1]. Firstly, 20 mg of perovskite was dissolved in 20 mL of 1 M HCl solution in a flask. Then, 3 mL of 2 M KI solution was added, the solution was transformed into a deep golden color; this solution was then titrated to a faint golden color with a 0.03 M $Na_2S_2O_3$. Then, 1 mL starch was added as an indicator

and the solution was titrated until it became colorless at the end, and oxygen vacancy content could be calculated from the obtained average valence state of B-site cations.

Working Electrodes Preparation:

10 mg catalyst and 10 mg carbon black were dispersed in 200 μL water, 700 μL isopropanol and 100 μL 5 wt.% Nafion by sonication for at least 3 h to form a homogeneous ink. The GCE were polished with alumina paste before using. The working electrode was then prepared by depositing 5 μL catalyst ink onto GCE, (catalyst loading ~ 0.255 mg cm^{-2}), and then the GCE was dried overnight in air at room temperature before testing.

Electrochemical Measurements:

All the electrochemical measurements were performed in 0.1 M KOH solution with a three-electrode system by using a Princeton instrument in a five-port electrochemical cell, which used an Ag/AgCl electrode as the reference electrode, a platinum gauze as the counter electrode and the catalyst dropped on a 0.196 cm^{-2} glassy carbon electrode (GCE, Pine Research Instrumentation) as the working electrode. Linear sweep voltammetry (LSV) was carried from 0.2 to 1.0 V versus Ag/AgCl (saturated KCl) at a scan rate of 10 mV s^{-1} and 1600 rpm. All potentials are iR-corrected with the equation of $E_{iR\text{-}corrected} = E_{applied\ potential\ vs\ RHE} - 0.196jR$ to compensate the loss from electrolyte resistance. Electrochemical impedance spectra (EIS) experiments were performed with the frequency scan range from 100 kHz to 0.1 Hz, the amplitude of the sinusoidal wave was 5 mV.

The electrochemically active surface area (ECSA) was estimated from the electrochemical double-layer capacitance (C_{dl}). The C_{dl} was determined from cyclic voltammograms (0.15 to 0.25 V vs. Ag/AgCl) at different scan rates (10, 20, 40, 60,

80, 100, 120, 140 mV s^{-1}, respectively). The double-layer current (j) is equal to the product of the v and C_{dl} based on $j = v \cdot C_{dl}$. Thus, the C_{dl} is then calculated according to: $C_{dl} = d(\Delta j(0.2\ V\ vs.\ Ag/AgCl))/2dv$. For the estimation of ECSA, a specific capacitance (C_S) value $C_S = 0.04$ mF cm^{-2} is adopted, and the ECSA is calculated according to: $ECSA = C_{dl}/C_S * S$, where S is surface area of the working electrode.

All potentials (vs Ag/AgCl) were calibrated to versus the reversible hydrogen electrode (RHE). The potential was calculated by the following equation:

$$E_{RHE} = E_{Ag/AgCl} + 0.951\ V$$

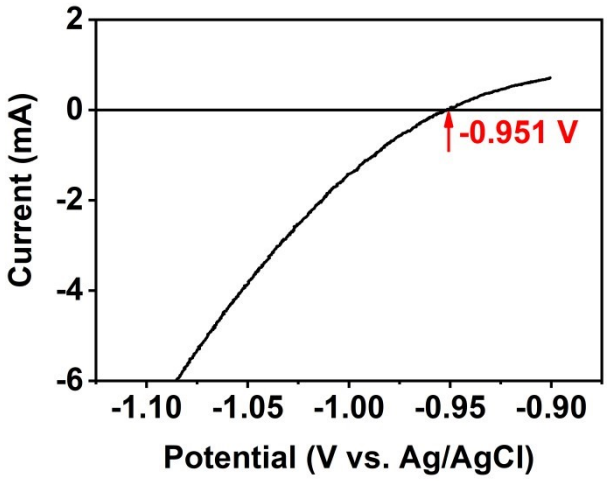

Figure S1. Potential calibration of the Ag/AgCl electrode in 0.1 M KOH solution.

DFT Calculations and FEA Stimulation:

DFT calculations were performed with the Perdew-Burke-Ernzerhof (PBE) exchange-correlation functional in a plane wave pseudopotential implementation using the Vienna ab initio simulation packages (VASP) [S2-S4]. A cutoff energy of 450 eV for the plane-wave basis set was employed. The DFT+U formalism was used to describe the localized (strongly correlated) 3d electrons in Cobalt and Nickel. For Co, $U_{Co} - J_{Co} = 3.3$ eV was used, For Ni, $U_{Ni} - Ni = 6.3$ eV was used. A Gamma centered k-

point sampling was adopted with a 15 Å vacuum to separate the slab perpendicular to the surface, where the bottom 3 layers were fixed as truncated bulk structure during structure optimization. The OH^- adsorption energy was calculated on LPBCN (110), where the convergence criteria for the residual force and energy during structure relaxation were set to 0.05 eV/Å and 1×10^{-5} eV, respectively.

FEA was performed by COMSOL Multiphysics 6.2. The OH^- density on the catalyst model surface was solved by the "Electric currents" module under the potential of 1.5 V. Electric field E and the electric potential V follow the equation: $\nabla\cdot J = Q_{j,\,v}$, $J = \sigma E + J_e$, $E = -\nabla V$. The electric conductivity of the electrode was taken to be 6.45×10^5 S m^{-1}. The electrolyte conductivity was taken to be 10 S m^{-1}. The diffusion coefficients D of the potassium ion, the hydroxide ion and the proton in water were 2.14×10^{-9} m^2 s^{-1}, 1.9×10^{-9} m^2 $s^{-1}$and 7.10×10^{-9} m^2 s^{-1}. The absolute temperature T was taken as 297.3 K. The OH^- density results were controlled by the following equations: $\nabla\cdot J_i + u\cdot\nabla c_i = R_i$, $J_i = -D_i\nabla c_i - Z_i u_{m,\,j} F c_i \nabla V$.

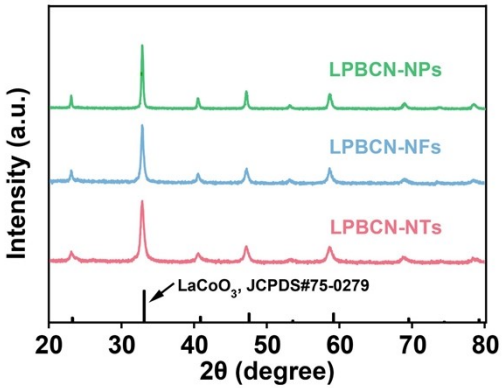

Figure S2. XRD patterns of LPBCN-NPs, LPBCN-NFs and LPBCN-NTs, respectively.

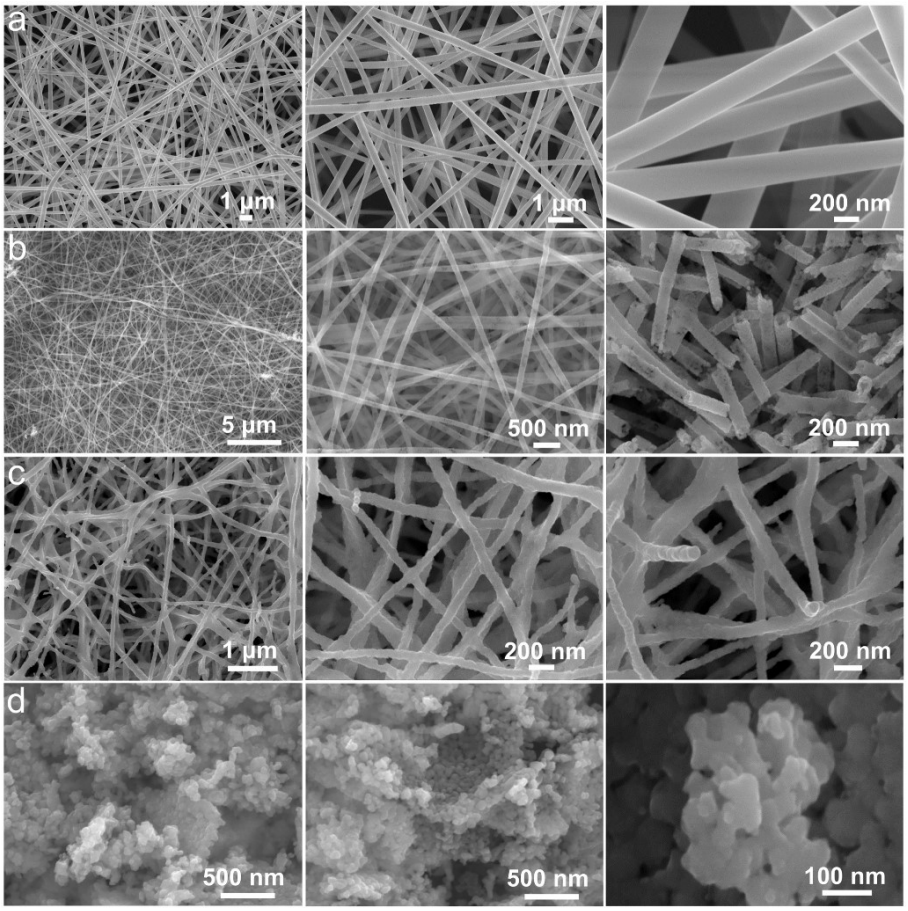

Figure S3. SEM images of a) precursor nanofibers of LPBCN-NTs, b) LPBCN-NTs, c) LPBCN-NFs, and d) LPBCN-NPs with different scales, respectively.

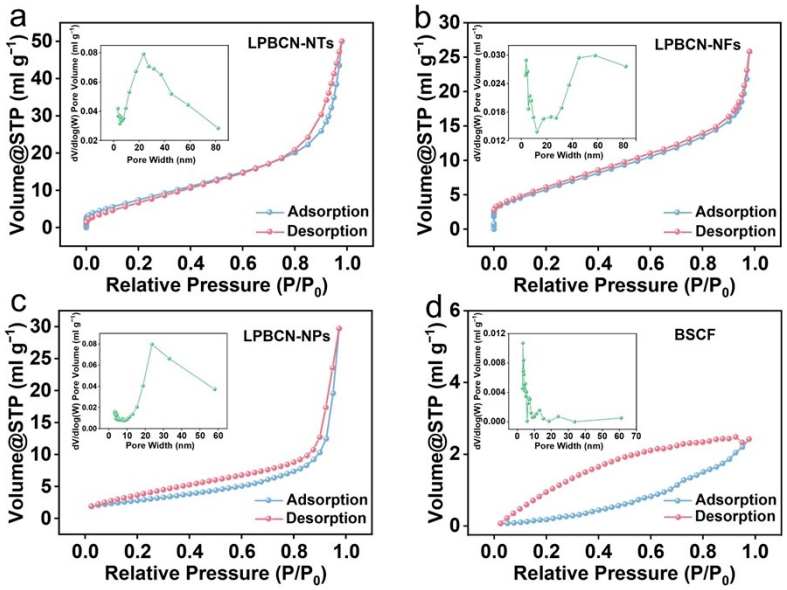

Figure S4. Nitrogen adsorption−desorption isotherms and pore size distribution (inset in each figure) of a) LPBCN-NTs, b) LPBCN-NFs, c) LPBCN-NPs and d) BSCF.

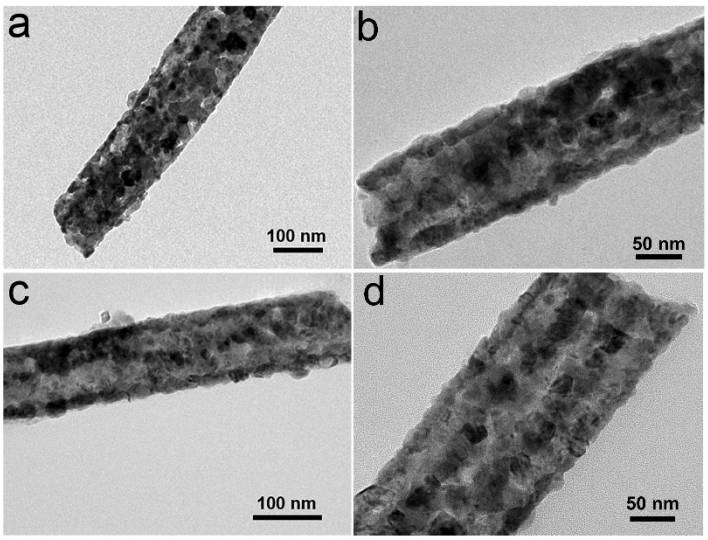

Figure S5. Low-magnification TEM images of LPBCN-NTs.

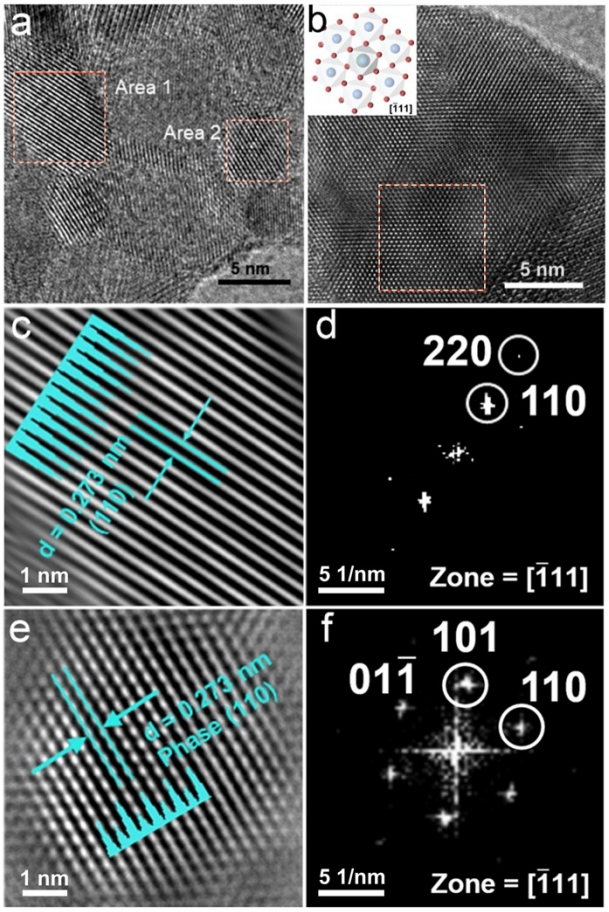

Figure S6. a) and b) High resolution TEM images of LPBCN-NTs. c) Magnified image and d) the corresponding FFT pattern of area 1 in figure (a). e) Magnified image and f) and the corresponding FFT pattern of area 2 in figure (c).

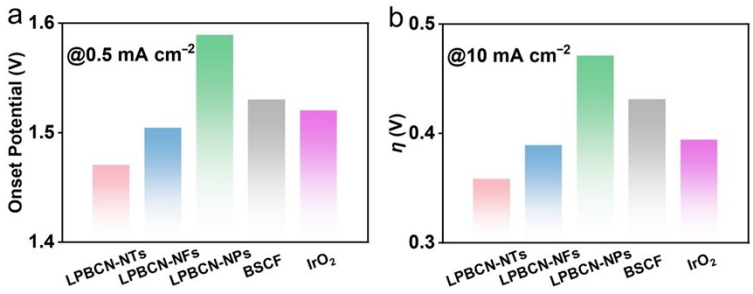

Figure S7. a) Onset Potential (@0.5 mA cm^{-2}) and b) η (@10 mA cm^{-2}) of LPBCN-NTs, LPBCN-NFs, LPBCN-NPs, BSCF and IrO_2.

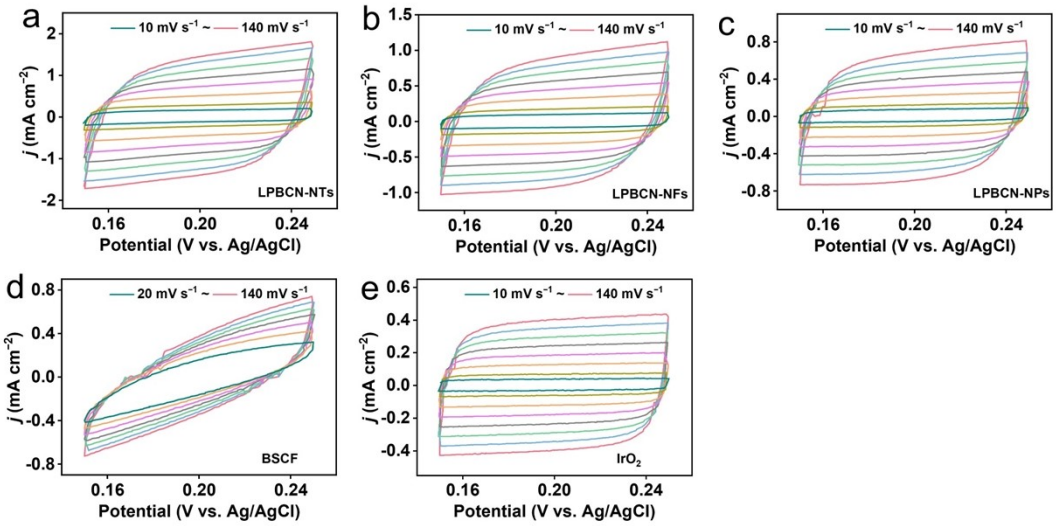

Figure S8. CV curves measured at different scan rates (from 10 mV s^{-1} to 140 mV s^{-1}) of a) LPBCN-NTs, b) LPBCN-NFs, c) LPBCN-NPs, d) BSCF and e) IrO_2, respectively.

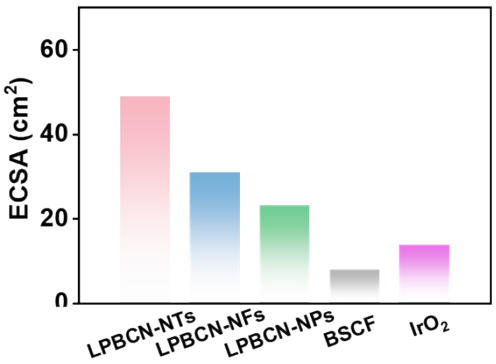

Figure S9. ECSAs of LPBCN-NTs, LPBCN-NFs, LPBCN-NPs, BSCF and IrO_2, respectively.

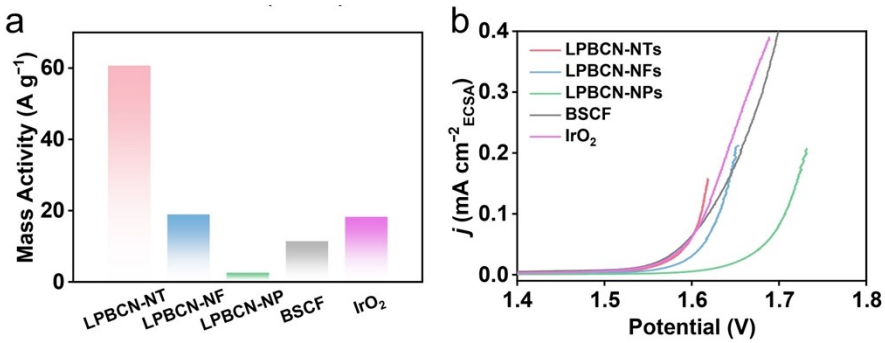

Figure S10. a) Mass activities at η = 0.38 V and ECSA-normalized LSV curves of LPBCN-NTs, LPBCN-NFs, LPBCN-NPs, BSCF and IrO_2, respectively.

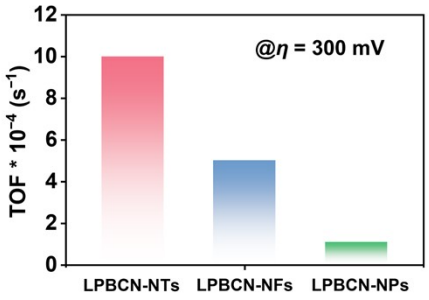

Figure S11. Calculated TOFs of LPBCN-NPs, LPBCN-NFs and LPBCN-NTs at η = 300 mV.

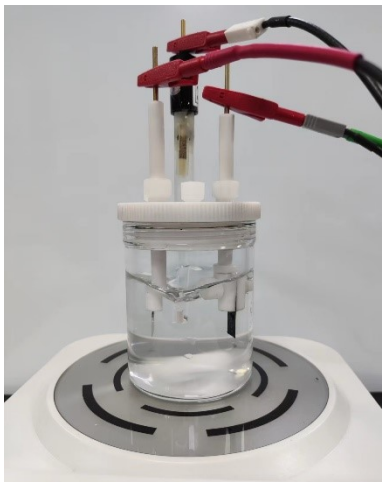

Figure S12. A carbon paper electrode in OER test based on a homemade cell.

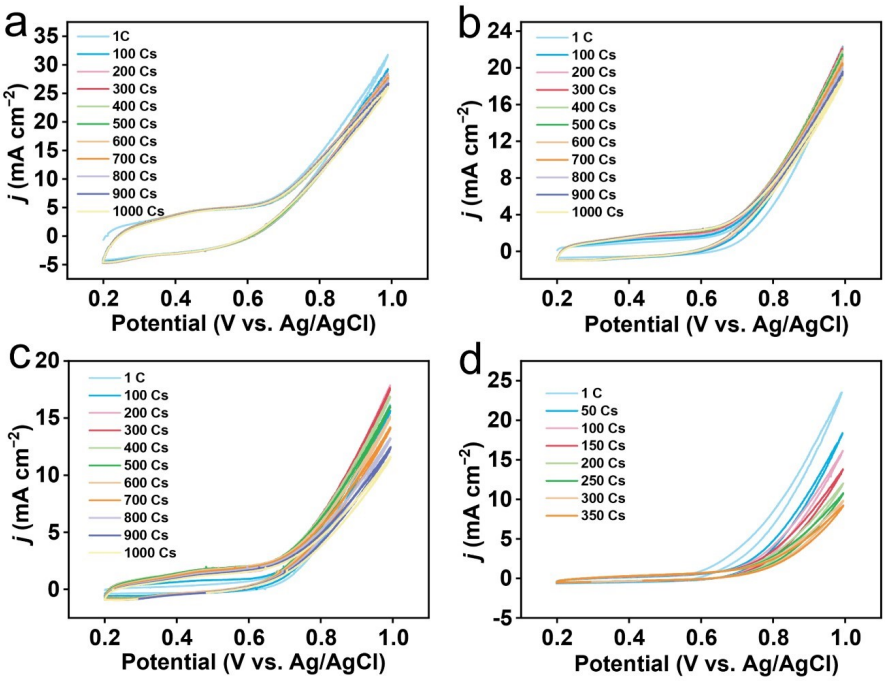

Figure S13. Continues CV tests of a) LPBCN-NTs with 1000 cycles, b) LPBCN-NFs with 1000 cycles, c) LPBCN-NPs with 1000 cycles and d) IrO_2 with 350 cycles.

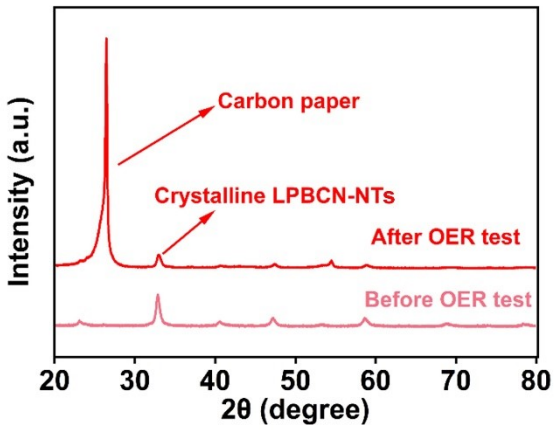

Figure S14. XRD patterns of LPBCN-NTs before and after CV test.

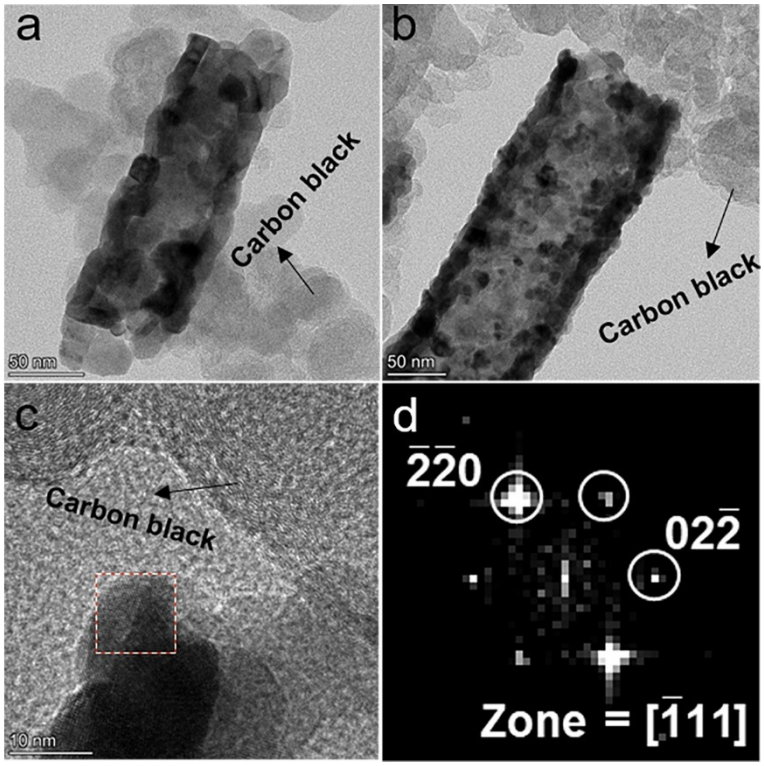

Figure S15. a) and b) TEM images, c) HRTEM image and d) the corresponding FFT pattern of LPBCN-NTs after OER test.

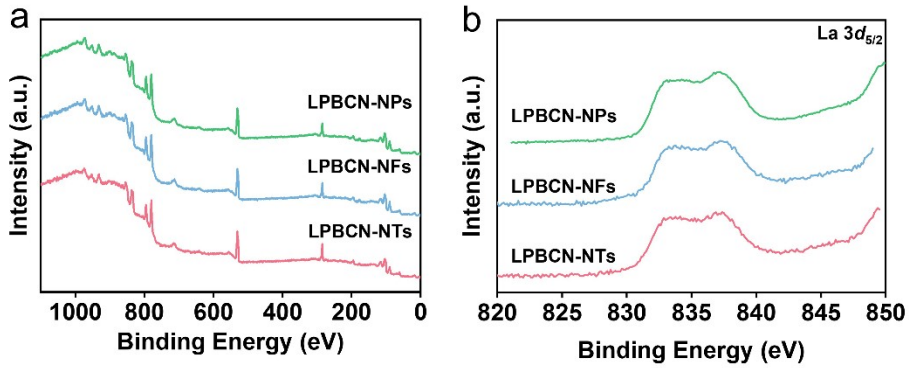

Figure S16. a) Survey XPS spectrum, b) La $3d_{5/2}$ XPS spectra of LPBCN-NTs, LPBCN-NFs and LPBCN-NPs.

Table S1. BET results for LPBCN-NPs, LPBCN-NFs, LPBCN-NTs and BSCF.

Electrocatalysts	Surface area (m^2 g^{-1})	Pore volume (cm^3 g^{-1})
LPBCN-NPs	10.425	0.04597
LPBCN-NFs	21.603	0.03995
LPBCN-NTs	30.48	0.0739
BSCF	1.65	0.0037

Table S2. A comparison of normalized OER activity for different perovskite catalysts.

Electrocatalysts	η@10 mA cm^{-2} (mV)	Tafel Slope (mV dec^{-1})	Ref.
Sm doped $LaCoO_3$ nanotubes	530	135.5	[S5]
$Co(OH)_2/Sr_2Fe_{1.5}Mo_{0.5}O_{6-\delta}$ nanofiber	384	71	[S6]
$La_{0.2}Sr_{0.8}FeO_{3-\delta}$	370	60.1	[S7]
$SrCo_{0.95}Si_{0.05}O_{3-\delta}$	417	66	[S8]
$La_{0.8}Sr_{0.2}Ti_{0.65}Fe_{0.35}O_3$	390	145	[S9]
$SrCoO_{2.8-\delta}S_{0.2}$	470	87.59	[S10]
$Sr(Co_{0.8}Fe_{0.2})_{0.95}P_{0.05}O_{3-\delta}$	400	82.8	[S11]
$La_{0.7}(Ba_{0.5}Sr_{0.5})_{0.3}Co_{0.8}Fe_{0.2}O_{3-\delta}$	480	97	[S12]
This study	358.8	71.46	-

Supplementary References

1 S. V. Porokhin, V. A. Nikitina, D. A. Aksyonov, D. S. Filimonov, E. M. Pazhetnov, I. V. Mikheev, and A. M. Abakumov, Mixed-cation perovskite $La_{0.6}Ca_{0.4}Fe_{0.7}Ni_{0.3}O_{2.9}$ as a stable and efficient catalyst for the oxygen evolution reaction, ACS Catal. 11 (2021), 8338–8348.

2 Perdew, J. P.; Burke, K.; Ernzerhof, M., Generalized gradient approximation made simple. Phys. Rev. Lett. 1996, 77 (18), 3865.

3 Kresse, G.; Furthmüller, J., Efficient iterative schemes for ab initio total-energy calculations using a plane-wave basis set. Phys. Rev. B 1996, 54 (16), 11169.

4 Kresse, G.; Hafner, J., Ab initio molecular dynamics for open-shell transition metals. Phys. Rev. B 1993, 48 (17), 13115.

5 Yu, Z. Y., Duan, Y., Kong, Y., Zhang, X. L., Feng, X. Y., Chen, Y., Wang, H., Yu, X., Ma, T., Zheng, X., Zhu, J., Gao, M. R., Yu, S. H., General synthesis of tube-like nanostructured perovskite oxides with tunable transition metal–oxygen covalency for efficient water electrooxidation in neutral media. J. Am. Chem. Soc., 144 (2022), 13163-13173.

6 B. He, K. Tan, Y. Gong, R. Wang, H. Wang and L. Zhao, Coupling amorphous cobalt hydroxide nanoflakes on $Sr_2Fe_{1.5}Mo_{0.5}O_{5+\delta}$ perovskite nanofibers to induce bifunctionality for water splitting, Nanoscale 12 (2020), 9048−9057.

7 S. She, J. Yu, W. Tang, Y. Zhu, Y. Chen, J. Sunarso, W. Zhou and Z. Shao, Systematic study of oxygen evolution activity and stability on $La_{1-x}Sr_xFeO_{3-\delta}$ perovskite electrocatalysts in alkaline media, ACS Appl. Mater. Interfaces 10 (2018), 11715−11721.

8 Y. Pan, X. Xu, Y. Zhong, L. Ge, Y. Chen, J. M. Veder, D. Guan, R. O'Hayre, M. Li, G. Wang, H. Wang, W. Zhou, Z. Shao, Direct evidence of boosted oxygen evolution over perovskite by enhanced lattice oxygen participation, Nat. Commun. 11 (2020) 2002.

9 Li, F., Mushtaq, N., Su, T., Cui, Y., Huang, J., Sun, M., Singh, M., Zhao, X., Maliutina, K., Zhang, Y., He, C., Yang, M., Zhu, B., Fan, L. NCNT grafted perovskite oxide as an active bifunctional electrocatalyst. Mater. Today Nano, 21 (2023), 100287.

10 Wang, X., Liu, H., Li, M., Li, J., Lu, Y., Wang, L., Wang, Z., Zhang, X., Ding, X., Modulation of electronic structure and oxygen vacancies of perovskites $SrCoO_{3-\delta}$ by sulfur doping enables highly active and stable oxygen evolution reaction. Electrochim. Acta, 390 (2021), 138872.

11 Zhang, W., Zhou, W., Zhang, Z., Chen, Z., Tan, S., Chen, D., Selective partial substitution of B-Site with phosphorus in perovskite electrocatalysts for highly efficient oxygen evolution reaction. ChemNanoMat, 5 (2019), 352-357.

12 J.-I. Jung, M. Risch, S. Park, M.G. Kim, G. Nam, H.-Y. Jeong, Y. Shao-Horn, J. Cho, Optimizing nanoparticle perovskite for bifunctional oxygen electrocatalysis, Energy Environ. Sci., 9 (2016) 176-183.